Diagnostic Capability of Three-Dimensional Macular Parameters for Glaucoma Using Optical Coherence Tomography Volume Scans

Alice C. Verticchio Vercellin,[1–4] Firas Jassim,[3,4] Linda Yi-Chieh Poon,[3–5] Edem Tsikata,[3,4] Boy Braaf,[4,6] Sneha Shah,[3,7] Geulah Ben-David,[3,4,8] Eric Shieh,[3,4,9] Ramon Lee,[3,4,10] Huseyin Simavli,[3,4,11] Christian J. Que,[3,4,12,13] Georgia Papadogeorgou,[14] Rong Guo,[4,15] Benjamin J. Vakoc,[4,6] Brett E. Bouma,[4,6] Johannes F. de Boer,[16,17] and Teresa C. Chen[3,4]

[1]University Eye Clinic, Istituto di Ricovero e Cura a Carattere Scientifico (IRCCS), Policlinico San Matteo, Pavia, Italy
[2]IRCCS-Fondazione Bietti, Rome, Italy
[3]Massachusetts Eye and Ear Infirmary, Department of Ophthalmology, Glaucoma Service, Boston, Massachusetts, United States
[4]Harvard Medical School, Boston, Massachusetts, United States
[5]Kaohsiung Chang Gung Memorial Hospital, Chang Gung University College of Medicine, Department of Ophthalmology, Kaohsiung, Taiwan
[6]Wellman Center for Photomedicine, Massachusetts General Hospital, Boston, Massachusetts, United States
[7]Johns Hopkins School of Medicine, Baltimore, Maryland, United States
[8]Sackler School of Medicine, Tel Aviv University, Tel Aviv, Israel
[9]Jules Stein Eye Institute, David Geffen School of Medicine, University of California, Los Angeles, California, United States
[10]University of Southern California Roski Eye Institute, Department of Ophthalmology, Keck School of Medicine, Los Angeles, California, United States
[11]Kudret Eye Hospital, Kadikoy, Istanbul, Turkey
[12]University of the East Ramon Magsaysay Memorial Medical Center, Quezon City, Philippines
[13]Romblon Provincial Hospital, Liwanag, Odiongan, Romblon, Philippines
[14]Harvard School of Public Health, Department of Biostatistics, Boston, Massachusetts, United States
[15]University of California, Los Angeles, Department of Internal Medicine, Los Angeles, California, United States
[16]LaserLaB Amsterdam, Department of Physics and Astronomy, Vrije Universiteit, The Netherlands
[17]Department of Ophthalmology, VU Medical Center, The Netherlands

Correspondence: Teresa C. Chen, Massachusetts Eye and Ear Infirmary, Glaucoma Service, 243 Charles Street, Boston, MA 02114, USA; teresa_chen@meei.harvard.edu.

PURPOSE. To compare the diagnostic capability of three-dimensional (3D) macular parameters against traditional two-dimensional (2D) retinal nerve fiber layer (RNFL) thickness using spectral domain optical coherence tomography. To determine if manual correction and interpolation of B-scans improve the ability of 3D macular parameters to diagnose glaucoma.

METHODS. A total of 101 open angle glaucoma patients (29 with early glaucoma) and 57 healthy subjects had peripapillary 2D RNFL thickness and 3D macular volume scans. Four parameters were calculated for six different-sized annuli: total macular thickness (M-thickness), total macular volume (M-volume), ganglion cell complex (GCC) thickness, and GCC volume of the innermost 3 macular layers (retinal nerve fiber layer + ganglion cell layer + inner plexiform layer). All macular parameters were calculated with and without correction and interpolation of frames with artifacts. The areas under the receiver operating characteristic curves (AUROC) were calculated for all the parameters.

RESULTS. The 3D macular parameter with the best diagnostic performance was GCC-volume-34, with an inner diameter of 3 mm and an outer of 4 mm. The AUROC for RNFL thickness and GCC-volume-34 were statistically similar for all regions (global: RNFL thickness 0.956, GCC-volume-34 0.939, P value = 0.3827), except for the temporal GCC-volume-34, which was significantly better than temporal RNFL thickness (P value = 0.0067). Correction of artifacts did not significantly change the AUROC of macular parameters (P values between 0.8452 and 1.0000).

CONCLUSIONS. The diagnostic performance of best macular parameters (GCC-volume-34 and GCC-thickness-34) were similar to or better than 2D RNFL thickness. Manual correction of artifacts with data interpolation is unnecessary in the clinical setting.

Keywords: spectral domain optical coherence tomography, diagnostic capability, macula, glaucoma

Glaucoma is the leading cause of irreversible blindness worldwide.[1] It is an optic neuropathy characterized by the progressive optic nerve head (ONH) cupping as well as degeneration of retinal ganglion cells and the loss of their axons, which comprise the retinal nerve fiber layer (RNFL).[2,3] Optical coherence tomography (OCT) allows for noninvasive quantitative imaging of these affected structures in order to facilitate the detection and monitoring of glaucoma.[4–6] Of these structures, the peripapillary RNFL thickness measurement is currently the most commonly utilized OCT parameter for clinical glaucoma assessments.[5–8]

In addition to the traditional RNFL thickness parameter, the macula has recently become a target for structural glaucoma analysis.[9–19] Approximately 50% of the over 1 million retinal ganglion cells (RGCs) contained in the human retina are concentrated within 4.5 mm of the fovea, and the macula is the only area where the ganglion cell layer is more than one cell layer thick (up to seven layers).[20] Spectral domain (SD) OCT has enabled the segmentation of the three innermost layers of the macular retina: the retinal nerve fiber layer, the ganglion cell layer (GCL), and the inner plexiform layer (IPL).[21–23] The RTVue SD-OCT platform (Optovue, Inc., Fremont, CA, USA) calls these 3 layers the ganglion cell complex (GCC). The Cirrus platform (software versions 6.0 or higher; Carl Zeiss Meditec, Inc., Dublin, CA, USA) analyzes the macular region with the ganglion cell analysis, which measures the combined thickness of two layers (i.e., the GCL and the IPL) or GCIPL. For the Spectralis HRA OCT platform (Heidelberg Engineering, Heidelberg, Germany), software for posterior pole asymmetry analysis (PPAA) is available to evaluate total retinal thickness in the macular region in a $30° \times 25°$ scan region, which was divided into an 8×8 grid. Some studies have even used the commercially available ETDRS (Early Treatment Diabetic Retinopathy Study) circles, which were designed for assessing diabetic disease and not glaucoma, to assess macular thickness in glaucoma patients.[24,25] For all of these 3 commonly used SD-OCT platforms, a literature review generally suggests that the current commercially available SD-OCT macular software has the same or worse diagnostic potential as the traditional RNFL thickness parameter.[24–38]

Because a review of the currently available macular software for glaucoma patients suggests that macular analysis is no better than the most commonly used RNFL thickness parameter,[24–38] this study had two specific aims. The first aim was to develop customized glaucoma software for macular analysis in the clinic to see if a macular parameter could be developed that is better than the traditional RNFL thickness parameter. For this novel software, we first acquired high density 6×6 mm macular volume scans and then used our custom-designed software to analyze the total retina and GCC retina for both macular thickness and volume parameters for six different-sized annular regions. The second aim of this study was to determine if SD-OCT macular analysis could be improved upon by manual correction of segmentation errors. The latter aim was stimulated by the hypothesis that a principle limitation of SD-OCT macular analysis is the high incidence of artifacts caused by segmentation errors. In the macula, it is difficult to correctly segment the inner retinal layers, because the difference in their scattering properties is relatively small.[39] High incidences of macular artifacts where found when Han and Jaffe analyzed macular volume scans of 88 eyes from 54 patients for image artifacts within each scan overall and within the center 1-mm area. Artifacts were considered clinically significant if they resulted in errors of more than 50 μm or more than 10% of retinal thickness or that caused a misdiagnosis of macular edema or retinal thinning. They found that 90.9% of 88 Spectralis HRA OCT scans had at least one artifact, and 37.5% (or 33 of 88 scans) had at least 1

artifact in the central 1 mm area.[39] Of the 88 scans, 8.0% (or 7 scans) had clinically significant artifacts.[39] Therefore, the first aim of our study was to compare the diagnostic capability of novel three-dimensional (3D) macular parameters (i.e., total and inner macular thickness and volume) to the traditional two-dimensional (2D) RNFL thickness measurements in a population of open angle glaucoma (OAG) patients and in a subgroup of subjects with early OAG. Then the secondary aim of this study was to determine if the diagnostic capability of 3D macular parameters can be improved upon with manual correction of artifacts.

MATERIALS AND METHODS

Participants and Examinations

All study subjects were recruited from the Glaucoma Service at the Massachusetts Eye and Ear Infirmary between April 2009 and July 2014, as a part of the prospective Spectral Domain OCT in Glaucoma (SIG) study, which was approved by the Massachusetts Eye and Ear Infirmary institutional review board. An informed consent form was obtained from all the subjects participating in the study. All methods adhered to the tenets of the Declaration of Helsinki for research involving human subjects, and the study was conducted in accordance with the Health Insurance Portability and Accountability Act. All study subjects underwent a complete eye examination by a glaucoma specialist (TCC), and this included history, visual acuity testing, refraction, Goldmann applanation tonometry, slit-lamp biomicroscopy, gonioscopy, ultrasonic pachymetry, and dilated ophthalmoscopy. All study subjects also had stereo disc photography (Visucam Pro NM; Carl Zeiss Meditec, Inc.), visual field (VF) testing (Swedish Interactive Threshold Algorithm 24–2 test of the Humphrey visual field analyzer 750i; Carl Zeiss Meditec, Inc.), and Spectralis OCT peripapillary RNFL thickness measurements (HRA/Spectralis software version 5.4.8.0, Heidelberg Engineering GmbH). The average RNFL thickness values for overall RNFL (360°), for each 90° quadrant (superior, temporal, inferior, and nasal), and for each sector [superior temporal (ST), superior nasal (SN), inferior temporal (IT), and inferior nasal (IN)] were recorded from the Spectralis OCT RNFL printouts.

Patients were included if they had a spherical equivalent between −5.0 and +5.0 diopters and a best-corrected visual acuity of 20/40 or better. Only patients with reliable VF testing were included, with less than 33% fixation losses, less than 20% false-positive results, and less than 20% false-negative results. Patients were excluded if they had discernible congenital anomalies of the anterior chamber, corneal scarring, or opacities, severe nonproliferative or proliferative diabetic retinopathy, VF loss attributable to a nonglaucoma condition, or a dilated pupil diameter of less than 2 mm.

Glaucoma patients were defined as having characteristic changes of the ONH with corresponding abnormal VF defects. The VF was considered to be abnormal if 3 or more contiguous test locations in the pattern standard deviation plot were depressed significantly at the $P < 0.05$ level with at least 1 at the $P < 0.01$ level on the same side of the horizontal meridian and if the VF defect corresponded to the optic nerve appearance.[40] Both primary and secondary OAG patients were included: 67 primary OAG patients, 14 pseudoexfoliation glaucoma patients, 13 normal tension glaucoma patients, and 7 pigmentary glaucoma patients. We did subanalysis on a subgroup of early OAG patients with VF mean deviations ranging from 0 to −6 dB.

Normal subjects were without ocular disease, except for mild cataracts, and had normal VF test results, as defined by a
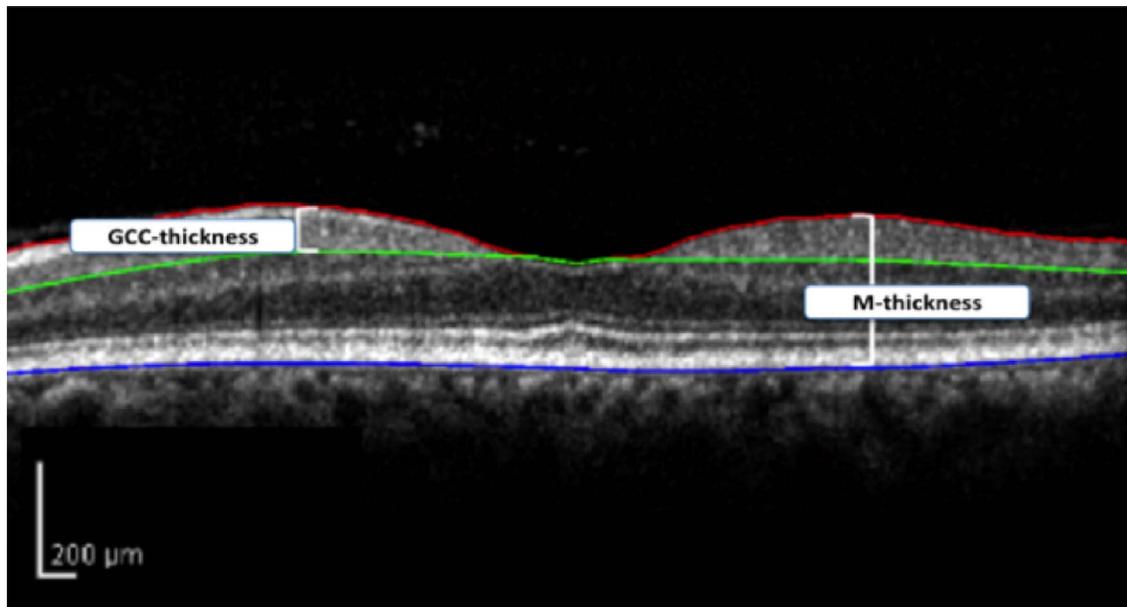
FIGURE 1. Example of an SD-OCT scan of the macula demonstrating segmentation of the three innermost retinal layers (GCC). GCC is comprised of three layers: the ganglion cell layer, the inner plexiform layer, and the retinal nerve fiber layer. The thickness of the three innermost retinal layers (GCC-thickness) is bound anteriorly by the *red line* (internal limiting membrane) and posteriorly by the *green line* (poster boundary of the inner plexiform layer). The total macular thickness (M-thickness) is bound anteriorly by the internal limiting membrane (*red line*) and posteriorly by the retinal pigment epithelium (*blue line*).

pattern standard deviation of more than 5% and glaucoma hemifield test results within normal limits.[41] If both eyes were eligible for the study, 1 eye was selected randomly by using the RANDBETWEEN (min, max) function in a spreadsheet program (Excel 2007; Microsoft Corp., Redmond, WA, USA). We defined "1" for the "min" and "2" for the "max." We ran the command = RANDBETWEEN (1,2) for every row of patients where both eyes were eligible. We picked the right eye for the result "1" and left eye for the result "2."

SD-OCT Macular Volumetric Study Protocol

After pupillary dilation, SD-OCT imaging was performed with the Spectralis OCT machine which utilizes an 870-nm super-luminescent diode source.[42,43] Spectralis OCT provides an automatic real-time (ART) function with an eye-tracking system that can increase image quality. With the ART function activated, multiple frames of the same scanning location are obtained. These data then are averaged for noise reduction, and eye-motion artifacts are reduced. Scans with signal strength of less than 15 dB (range: 0–40) were excluded from the analysis.[44] In addition, the criteria for determining adequate scan quality were as follows: a clear fundus image with good optic disc and scan area visibility before and during image acquisition, overlay of volume scan visible and without interruptions, and a continuous scan pattern without missing or blank areas.

The Spectralis OCT macular volume scan encompassed a $20° × 20°$ field that was $6 × 6$ mm. We obtained 193 B-scans per volumetric scan and were taken with the high-speed rate and ART set at 3.

Analysis of SD-OCT Macular Volume Scans

Analysis of OCT macular volume scans was performed by a custom-built program written in a computing environment (MATLAB; MathWorks, Inc., Natick, MA, USA). Figure 1 shows how the 193 B-scans were segmented by the software to determine the inner macular region (GCC = ganglion cell layer, inner plexiform layer, retinal nerve fiber layer) and the entire macular region (M). The software automatically segmented the inner limiting membrane (ILM, red line), the posterior boundary of GCC (inner plexiform layer, green line), and the RPE (blue line). The fovea was identified automatically by the software or, when needed, manually corrected by one of the authors (ACVV).

Figure 2 shows the six different-sized annular regions, which were used to calculate thickness and volume for both the entire macular retina (M) and the inner three layers of the macular retina (GCC). The six different-sized annuli included four annuli with widths of 1 mm, while the other 2 annuli had larger widths. Of the annular regions with a 1-mm width, the smallest annulus had an inner diameter of 1 mm and outer diameter of 2 mm, the next largest annulus had diameters of 2 and 3 mm, the next largest annulus had diameters of 3 and 4 mm, and the largest annuli had diameters of 4 and 5 mm. The two remaining annuli had diameters of 1 and 4 mm and diameters of 1 and 5 mm. For all six different-sized annuli, M-thickness, M-volume, GCC-thickness, and GCC-volume were calculated. Thickness values were in µm, and volume values were in mm³. For terminology of M and GCC parameters, the inner and outer diameter lengths are placed after the parameter. So, for example, M-volume-34 represents the total macular volume for an annulus with inner diameter of 3 mm and outer diameter of 4 mm. Another example is GCC-thickness-15, which is the thickness of the inner three layers of the macular retina within an annulus of inner diameter 1 mm and outer diameter 5 mm.

Thickness and volume of the total macula and of GCC in each annulus were calculated for 360° (global), for each 90° quadrant (superior, temporal, inferior and nasal), and for 4 sectors (superior nasal [SN], superior temporal [ST], inferior temporal [IT], inferior nasal [IN]).

All 193 B-scans for each subject were then checked for algorithm artifacts and errors by one of the authors (ACVV). Artifacts were broadly categorized into two types: segmenta-
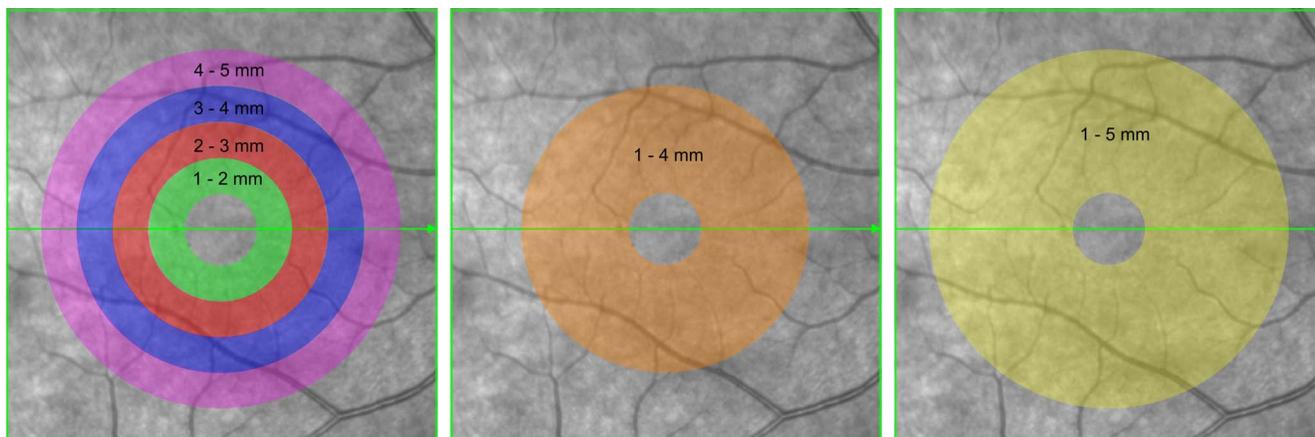
FIGURE 2. The six different-sized annuli, which were used to calculate the macular parameters, are depicted and superimposed on an en face SD-OCT macular image. This figure specifically explains the terminology used for the six macular volume (M-volume) annuli: the smallest annulus (M-volume-12) is delimited by *circles* of diameters 1.00 and 2.00 mm (*green area* in the *left image*); the second annulus (M-volume-23) by circles of diameters 2.00 and 3.00 mm (*red area* in the *left image*); the third annulus (M-volume-34) by 3.00 and 4.00 mm (*blue area* in the *left image*); the fourth annulus (M-volume-45) by 4.00 and 5.00 mm (*violet area* in the *left image*); the fifth annulus (M-volume-14) by 1.00 and 4 mm (*orange area* in the *center image*), and the largest annulus (M-volume-15) by 1.00 and 5 mm (*yellow area* in the *right image*).

tion artifacts or acquisition artifacts. A segmentation artifact includes either misidentification or no segmentation of the ILM, GCC, or RPE. Acquisition artifacts included the following types: (1) jump or out-of-register artifacts, where the scan was shifted up or down and out of the scan display box, (2) cut edge artifact, where part of the displayed retinal cross-section was truncated, (3) absence of image artifact, where the entire B-scan was missing, and (4) mirror artifact. The artifact rates were calculated by dividing the number of B-scans with artifacts (numerator) by the total number of B-scans per each volume scan (denominator). The percentage of volume scans with at least one B-scan artifact was also calculated.

Scans containing artifacts were manually deleted, and the software then again calculated the aforementioned measurements with interpolation of deleted frames.

Statistical Analysis

Statistical analyses were performed using R 3.2.3 and R packages AUROC 0.3.0, pROC 1.9.1. Demographic characteristics of the normal and glaucoma groups were compared using Fisher's exact test for categorical variables and two-sided Student's *t*-test for continuous variables. Only one eye per patient was included for statistical analyses.

The artifact rates per B-scan were compared between normal and glaucoma patients using χ^2 test. Two sample *t*-tests were performed to compare the macular parameters before and after interpolation for the normal and glaucoma subject data.

Areas under the receiver operating characteristic (AUROC) curves were calculated for peripapillary RNFL thickness, M-thickness, GCC-thickness, M-volume, and GCC-volume for discriminating glaucoma from healthy patients for 360° (global), for each 90° quadrant, and for all eight sectors (NS, SN, ST, TS, IT, TI, IN, NI). Sensitivity, specificity, positive predictive value (PPV), negative predictive value (NPV), positive likelihood ratio (PLR), and negative likelihood ratio (NLR) were calculated for each parameter using the cutoff value based on the maximum value of the Youden index (J), which is equal to the maximum of (Sensitivity + Specificity – 1). Pairwise comparisons of receiver operating characteristic (ROC) curves were performed between all parameters before and after interpolation of the data. Delong's method was performed for comparison of ROC curves. Values of $P < 0.05$ established statistical significance. The *P* values reported are false discovery rate corrected (FDR-corrected) to control for multiple testing where applicable. Results are expressed as mean ± standard deviation, unless otherwise stated.

RESULTS

A total of 162 subjects were initially enrolled into the study. Out of this group, four subjects were excluded, because these patients were not able to complete the OCT volume scans. Table 1 lists the demographic characteristics of the remaining 158 patients who were included in the study (101 OAG

TABLE 1. Demographics of the Normal Subjects and OAG Patients With SD-OCT Macular Volume Scans*

	Normal Subjects	OAG Patients	P Value
Eyes, *n*	57	101	
Number of eyes, right/left	31/26	51/50	0.7405
Sex, female/male	39/18	47/54	0.0123
Age, y	54.1 ± 15.5	68.2 ± 11.9	<0.0001
Refractive error spherical equivalent, diopters (D)	−0.36 ± 1.75	−0.67 ± 1.81	0.3065
Visual field MD, dB	−1.41 ± 1.95	−11.85 ± 7.50	<0.0001
Visual field PSD dB	1.52 ± 0.30	8.41 ± 3.20	<0.0001

PSD, pattern standard deviation.
* Results are expressed as the mean ± SD unless otherwise indicated. Demographic characteristics of the normal and glaucoma groups were compared using Fisher's exact test for categorical variables and two-sided Student's *t*-test for continuous variables. Values of $P < 0.05$ established statistical significance.

TABLE 2. Frequency of Artifacts Seen in 3D SD-OCT Macular Volume Scans in Normal Subjects Versus OAG Patients

	Normal Subjects (Percentage of Artifacts per B-scan), %*	OAG Patients (Percentage of Artifacts per B-scan), %*	*P* Value
Segmentation artifact of the posterior GCC boundary	13.5	19.8	<0.0001
Segmentation artifact of the RPE	3.5	4.3	0.0017
Segmentation artifact of the ILM	2.6	4.4	<0.0001
Acquisition artifact of the posterior GCC boundary†	0.1	0.5	<0.0001
Acquisition artifact of the ILM†	0.1	0.5	<0.0001
Acquisition artifact of the RPE†	0.1	0.4	<0.0001

GCC refers to the three innermost retinal layers: ganglion cell layer (G), inner plexiform layer (I), and retinal nerve fiber layer (R). The artifact rates per B-scan were compared between normal subjects and glaucoma patients using χ^2 test. Values of $P < 0.05$ established statistical significance.

* Percentages of artifacts are calculated per B-scan and not per volume scan. There are 193 B-scans per volume scan, and 100% of volume scans had at least 1 B-scan with an artifact.

† Acquisition artifacts include jump artifacts, cut edge artifacts, missing image artifacts, and reflection error artifacts.

patients, of which 29 had early OAG; and 57 healthy subjects). The glaucomatous subjects were older (68.2 ± 11.9 years) compared to the normal subjects (54.1 ± 15.5 years, $P < 0.0001$). The glaucoma patients had significantly lower mean deviations and higher pattern standard deviations compared to healthy subjects ($P < 0.0001$).

For the different size annuli (Fig. 2), larger annuli extended beyond the 6 × 6 mm scanned region a higher percentage of the time: annulus with diameters 1 and 2 mm (0% of the time outside the scanned region), annulus with diameters 2 and 3 mm (0.2%), annulus with diameters 3 and 4 mm (0%), and annulus with diameters 4 and 5 mm (0.9%).

We found 100% of macular volume scans had at least one B-scan with an artifact. Table 2 shows that the most common type of segmentation artifact was segmentation errors of the posterior border of the GCC, and that this artifact was significantly more common in OAG compared to healthy subjects (19.8% vs. 13.5%, $P < 0.0001$, Table 2). Acquisition artifacts were less frequent than segmentation artifacts (0.1%–0.5% vs. 2.6%–19.8%, Table 2), but acquisition artifacts were also significantly more common in OAG compared to healthy subjects (0.4% to 0.5% vs. 0.1%, $P < 0.0001$, Table 2). The algorithm correctly located the foveal center in all but 19 patients, who required manual centration of the annuli.

Table 3 shows that the overall global RNFL was thinner for the glaucoma eyes compared to the normal eyes (58.3 ± 15.4 μm vs. 94.8 ± 12.1 μm, $P < 0.0001$). The RNFL was thinner for glaucoma versus normal subjects for all quadrants and sectors (Table 3).

Although GCC-volume and M-volume (Table 4) and GCC-thickness and M-thickness values (Table 5) for all annuli were calculated before and after manual deletion with interpolation

of artifacts, the AUROC curve values for all parameters for all annuli before and after interpolation did not significantly differ (P values between 0.8452 and 1.0000, data not shown). Therefore, only values from before interpolation were displayed in Tables 4 and 5. For all annuli sizes and for all global parameters (M-thickness, M-volume, GCC-thickness, GCC-volume, Tables 4 and 5), values were lower for glaucoma eyes compared to normal eyes (P values all < 0.0001). The mean difference of the global M-thickness values for before and after interpolation was 1.831 ± 20.658 μm, of the global M-volume was 0.000 ± 1.832 mm³, of the global GCC-thickness was 0.280 ± 1.967 μm, and of the global GCC-volume was 0.005 ± 0.037 mm³.

In Tables 6 and 7, we listed the volume parameters (GCC-volume and M-volume) and in Supplementary Tables S1 and S2 the thickness parameters (GCC-thickness and M-thickness) for all glaucoma patients. In Tables 8 and 9, we listed the volume parameters (GCC-volume and M-volume) and in Supplementary Tables S3 and S4 the thickness parameters (GCC-thickness and M-thickness) for the subgroup of patients with early glaucoma.

Comparison of AUROC values between peripapillary RNFL thickness and GCC-volume (Table 6) and M-volume (Table 7) for all six annuli sizes are shown. The AUROC value for overall RNFL thickness was 0.956. However, for RNFL thickness, the best AUROC value for quadrants and sectors was the inferior quadrant (0.960), followed by the IT sector (0.957), superior quadrant (0.938), and ST sector (0.935). For GCC-volume parameters, annular region GCC-volume-34 achieved the best combination of both best diagnostic performance and most annular scans being within the 6 × 6 mm² square scanned region the highest percentage of the time (100%). The AUROC

TABLE 3. RNFL Thickness Values for the Normal Subjects Versus OAG Patients Using SD-OCT

RNFL Thickness Location	Normal Subjects RNFL Thickness, Mean ± SD, μm	OAG Patients RNFL Thickness, Mean ± SD, μm	*P* Value
Global	94.8 ± 12.1	58.3 ± 15.4	<0.0001
Inferior	123.3 ± 19.9	63.7 ± 23.0	<0.0001
Superior	114.6 ± 19.9	69.8 ± 20.6	<0.0001
Nasal	71.3 ± 13.8	49.8 ± 17.3	<0.0001
Temporal	69.6 ± 13.9	49.6 ± 16.7	<0.0001
IT	138.4 ± 23.9	65.1 ± 30.0	<0.0001
IN	108.3 ± 27.0	62.4 ± 22.4	<0.0001
ST	129.5 ± 23.2	75.0 ± 26.3	<0.0001
SN	99.9 ± 22.6	64.5 ± 21.9	<0.0001

Results are expressed as the mean ± SD unless otherwise indicated. Student's *t*-test was performed and values of $P < 0.05$ established statistical significance.

TABLE 4. GCC-Volume and M-Volume for Normal Subjects Versus OAG Patients Using SD-OCT Macular Volume Scans

Macular Volume Parameters	Normal Subjects (Mean ± SD mm^3)	OAG Patients (Mean ± SD mm^3)	P Value
GCC-volume-12	0.248 ± 0.025	0.192 ± 0.042	<0.0001
GCC-volume-23	0.480 ± 0.043	0.358 ± 0.071	<0.0001
GCC-volume-34	0.621 ± 0.059	0.458 ± 0.085	<0.0001
GCC-volume-45	0.724 ± 0.071	0.537 ± 0.095	<0.0001
GCC-volume-14	1.348 ± 0.111	1.007 ± 0.191	<0.0001
GCC-volume-15	2.082 ± 0.171	1.549 ± 0.280	<0.0001
M-volume-12	0.805 ± 0.039	0.750 ± 0.055	<0.0001
M-volume-23	1.365 ± 0.063	1.249 ± 0.086	<0.0001
M-volume-34	1.786 ± 0.087	1.626 ± 0.108	<0.0001
M-volume-45	2.137 ± 0.102	1.944 ± 0.126	<0.0001
M-volume-14	3.956 ± 0.174	3.626 ± 0.240	<0.0001
M-volume-15	6.107 ± 0.263	5.575 ± 0.353	<0.0001

Results are expressed as the mean ± standard deviation (SD) unless otherwise stated. Results are also expressed before interpolation of data for annular regions of varying sizes centered on the fovea. Student's *t*-test was performed and values of $P < 0.05$ established statistical significance.

value for global GCC-volume-34 was 0.939, which was similar to global RNFL thickness (P value = 0.3827). For GCC-volume-34, the best AUROC curve value for all quadrants and sectors was the temporal quadrant (0.947), which was significantly better than temporal RNFL (P value = 0.0067). After the temporal GCC-volume-34, best quadrants and sectors were inferior quadrant GCC-volume-34 (0.929) followed by the IT GCC-volume-34 (0.920, Table 6). Only the AUROC for the temporal quadrants for GCC-volume-23, GCC-volume-34, GCC-volume-45, GCC-volume-14 and GCC-volume-15 were significantly higher than corresponding RNFL quadrants (i.e., all P values were between 0.0045 and 0.0161, Table 6). The AUROC for the temporal M-volume-23, M-volume-34, M-volume-45, M-volume-14, and M-volume-15 were also higher but not significantly higher compared to corresponding RNFL thickness regions (i.e., all P values were between 0.5287 and 0.6534, Table 7). In all the other quadrants and sectors, the diagnostic performance of RNFL thickness was either significantly better or similar to the macular parameters (Tables 6, 7).

In contrast, for the nine regions (global, quadrant, and sector), Table 7 shows that AUROC curve values for five regions for M-volume-34 were significantly worse than RNFL thickness and for the four regions statistically similar to RNFL thickness. For the best M-volume annulus (i.e., M-volume-34), the AUROC value for overall M-volume-34 was 0.877 (i.e., significantly worse than global RNFL thickness AUROC = 0.956, P value = 0.0051, Table 7). Best regions for M-volume-34 were IT sector (0.885), temporal quadrant (0.885), and inferior quadrant (0.875), with inferior and IT M-volume-34 being

significantly worse than the corresponding regions for RNFL thickness (P values = 0.0041 for inferior quadrant, and 0.0067 for IT sector, Table 7). Therefore, in summary, inner retina parameter GCC-volume-34 had better diagnostic capability compared to total retina parameter M-volume-34 (Tables 6, 7), and total retina parameter (e.g., M-volume) had the same or worse diagnostic capability as RNFL thickness.

The AUROC of GCC-volume were significantly higher compared to M-volume in all the corresponding regions (i.e., all P values were between 0.0001 and 0.0445), except for the annuli between 1 and 2 mm (superior and nasal quadrants, NS, SN, ST, TS, TI, and NI sectors), between 2 and 3 mm (NI sector), and between 1 and 4 mm (nasal quadrant, NS sector), where the AUROC for GCC-volume were higher but statistically similar compared to M-volume (i.e., all P values were between 0.0521 and 0.1715). For the subgroup of 29 patients with early glaucoma (VF MD: 0 to −6 dB), comparisons of AUROC values between peripapillary RNFL thickness and GCC-volume (Table 8) and M-volume (Table 9) are shown. The AUROC value for overall RNFL thickness was 0.934. For RNFL thickness, the best AUROC values for quadrants and sectors were for the inferior quadrant (0.937), followed by the IT sector (0.919), superior quadrant (0.882), and ST sector (0.872). The AUROC value for global GCC-volume-34 was 0.901, which was similar to global RNFL thickness (0.934, P = 0.4409). The best AUROC curve value for GCC-volume-34 was the temporal quadrant (0.932), which was significantly better than temporal RNFL thickness (AUROC = 0.740, P = 0.0139), followed by the inferior quadrant (0.896), and by the IT sector (0.892, Table 8). For the

TABLE 5. GCC- and M-Thickness for Normal Subjects Versus OAG Patients Using SD-OCT Macular Volume Scans

Macular Thickness Parameters	Normal Subjects, Mean ± SD, μm	Glaucoma Patients, Mean ± SD, μm	P Value
GCC-thickness-12	103.368 ± 10.125	80.604 ± 17.520	<0.0001
GCC-thickness-23	120.632 ± 10.538	90.131 ± 17.656	<0.0001
GCC-thickness-34	111.772 ± 10.349	82.634 ± 15.222	<0.0001
GCC-thickness-45	101.593 ± 9.710	75.500 ± 13.433	<0.0001
GCC-thickness-14	114.455 ± 9.402	85.444 ± 16.214	<0.0001
GCC-thickness-15	110.428 ± 9.062	82.158 ± 14.868	<0.0001
M-thickness-12	335.421 ± 15.802	314.010 ± 21.689	<0.0001
M-thickness-23	342.912 ± 15.154	314.677 ± 20.862	<0.0001
M-thickness-34	321.263 ± 14.920	293.317 ± 19.258	<0.0001
M-thickness-45	299.630 ± 13.305	273.117 ± 17.625	<0.0001
M-thickness-14	335.777 ± 14.756	307.764 ± 20.343	<0.0001
M-thickness-15	323.976 ± 13.948	295.739 ± 18.749	<0.0001

Results are expressed as the mean ± SD unless otherwise stated. Results are also expressed before interpolation of data for annular regions of varying sizes centered on the fovea. Student's *t*-test was performed and values of $P < 0.05$ established statistical significance.

TABLE 6. Comparison of the Diagnostic Capabilities of RNFL Thickness vs. GCC-Volume Parameters Using SD-OCT

Location	RNFL Thickness AUROC	GCC-Volume-12 AUROC (*P* value)*	GCC-Volume-23 AUROC (*P* value)*	GCC-Volume-34 AUROC (*P* value)*	GCC-Volume-45 AUROC (*P* value)*	GCC-Volume-14 AUROC (*P* value)*	GCC-Volume-15 AUROC (*P* value)*
Global	0.956	0.872 (0.0126)*	0.924 (0.1686)	0.939 (0.3827)	0.950 (0.8979)	0.934 (0.3171)	0.944 (0.6776)
Inferior	0.960	0.851 (0.0057)*	0.906 (0.0276)*	0.929 (0.1276)	0.940 (0.2988)	0.922 (0.0802)	0.936 (0.2697)
Superior	0.938	0.838 (0.0137)*	0.888 (0.1267)	0.908 (0.3218)	0.928 (0.7357)	0.903 (0.2846)	0.918 (0.5287)
Nasal	0.836	0.783 (0.3676)	0.848 (0.8113)	0.864 (0.5472)	0.884 (0.2317)	0.856 (0.6598)	0.873 (0.3906)
Temporal	0.859	0.897 (0.4540)	0.939 (0.0161)*	0.947 (0.0067)*	0.950 (0.0057)*	0.950 (0.0067)*	0.954 (0.0045)*
IT	0.957	0.857 (0.0096)*	0.906 (0.0496)*	0.920 (0.1583)	0.929 (0.2634)	0.920 (0.1369)	0.932 (0.3218)
IN	0.909	0.833 (0.1019)	0.886 (0.5299)	0.915 (0.8423)	0.925 (0.5592)	0.910 (0.9916)	0.925 (0.5592)
ST	0.935	0.838 (0.0168)*	0.884 (0.1464)	0.894 (0.2507)	0.908 (0.4908)	0.897 (0.2881)	0.908 (0.4718)
SN	0.869	0.832 (0.4908)	0.878 (0.8392)	0.894 (0.5592)	0.903 (0.4256)	0.891 (0.5871)	0.907 (0.3725)

* *P* values indicate that there are statistically significant differences (*P* < 0.05) between RNFL thickness and GCC-volume AUROC. Delong's method was performed for comparison of AUROC curves. Values of *P* < 0.05 established statistical significance. The *P* values reported are false discovery rate corrected (FDR-corrected) to control for multiple testing.

best M-volume annulus (i.e., M-volume-34), the AUROC value for overall M-volume 34 was 0.806 (i.e., significantly worse than global RNFL thickness AUROC 0.934, *P* = 0.0438, Table 9). The best regions for M-volume-34 were IT sector (0.840), temporal quadrant (0.835), and inferior quadrant (0.816). Inferior M-volume-34 was significantly worse than the corresponding region for RNFL thickness (*P* = 0.0129), while all the other regions (superior, nasal, temporal quadrants, and IN, IT, SN and ST sectors), were statistically similar to RNFL thickness (i.e., all *P* values were between 0.1022 and 0.8785, Table 9).

In Tables 6 and 7, 2D RNFL thickness parameters were compared to 3D volume parameters (GCC-volume and M-volume). We compared 2D RNFL thickness parameters to 2D thickness parameters (GCC-thickness and M-thickness) for all glaucoma patients (Supplementary Tables S1, S2) and for the subgroup of patients with early glaucoma (Supplementary Tables S3, S4). Per AUROC curve values, the diagnostic ability of 2D RNFL thickness values versus 3D GCC and macular volume parameters were similar to comparisons between 2D RNFL thickness values and 2D GCC and macular thickness parameters except for the following: 3D nasal M-volume-12 was similar to 2D nasal RNFL thickness, while 2D nasal M-thickness-12 was significantly worse than 2D nasal RNFL thickness (Tables 7, Supplementary Table S2); for the subgroup of patients with early glaucoma, 3D inferior GCC-volume-12 was significantly worse than 2D inferior RNFL thickness, while 2D inferior GCC-thickness-12 was similar to 2D inferior RNFL thickness (Table 8, Supplementary Table S3); 3D global M-volume-34 was significantly worse compared to 2D global RNFL thickness, while 2D M-thickness-34 was comparable to 2D global RNFL thickness; 3D inferior M-volume-45 was significantly worse than 2D inferior RNFL thickness, while 2D inferior M-thickness-45 was comparable to 2D inferior RNFL thickness (Table 9, Supplementary Table S4). Otherwise, *P* values were similar when comparing AUROC curve values between 3D GCC-volume-34 (the best 3D macular parameter) and 2D GCC-thickness-34 (Tables 6, 8, Supplementary Tables S1, S3).

DISCUSSION

In our study, we used custom-designed macular software to calculate data from high density volumetric macular scans to evaluate the diagnostic performance of total macular and inner macular (GCC) thickness and volume. This study showed that the best 3D macular parameter, GCC-volume-34, had the same or better diagnostic capability as the traditional 2D peripapillary RNFL thickness parameter (i.e., temporal GCC-volume-34 being better than temporal RNFL thickness, both for all OAG patients, *P* = 0.0067, Table 6 as well as in an early OAG subgroup of patients, *P* = 0.0139, Table 8). GCC-volume parameters were the same or significantly better than M-volume parameters. Also, to our knowledge, this is the first study that demonstrates that manual deletion of B-scans with artifacts and subsequent interpolation of data did not increase the diagnostic performance of macular parameters, indicating that artifacts in 3D volume scans do not require manual correction in the clinic. This is significant, because this study

TABLE 7. Comparison of the Diagnostic Capabilities of RNFL Thickness Versus M-Volume Parameters Using SD-OCT

Location	RNFL Thickness AUROC	M-Volume-12 AUROC (*P* value)*	M-Volume-23 AUROC (*P* value)*	M-Volume-34 AUROC (*P* value)*	M-Volume-45 AUROC (*P* value)*	M-Volume-14 AUROC (*P* value)*	M-Volume-15 AUROC (*P* value)*
Global	0.956	0.799 (0.0006)*	0.862 (0.0053)*	0.877 (0.0051)*	0.891 (0.0196)*	0.865 (0.0048)*	0.887 (0.0158)*
Inferior	0.960	0.772 (0.0002)*	0.857 (0.0041)*	0.875 (0.0041)*	0.890 (0.0154)*	0.860 (0.0041)*	0.879 (0.0067)*
Superior	0.938	0.802 (0.0045)*	0.838 (0.0088)*	0.847 (0.0092)*	0.864 (0.0241)*	0.842 (0.0091)*	0.857 (0.0158)*
Nasal	0.836	0.743 (0.1055)	0.798 (0.5048)	0.813 (0.6365)	0.833 (0.9843)	0.810 (0.6021)	0.827 (0.8734)
Temporal	0.859	0.833 (0.6163)	0.876 (0.6534)	0.885 (0.5334)	0.880 (0.5592)	0.885 (0.5299)	0.883 (0.5287)
IT	0.957	0.763 (0.0002)*	0.863 (0.0048)*	0.885 (0.0067)*	0.888 (0.0245)*	0.869 (0.0057)*	0.884 (0.0108)*
IN	0.909	0.762 (0.0053)*	0.840 (0.0802)	0.848 (0.1108)	0.871 (0.4009)	0.844 (0.1071)	0.862 (0.2886)
ST	0.935	0.798 (0.0041)*	0.828 (0.0078)*	0.828 (0.0067)*	0.845 (0.0158)*	0.835 (0.0096)*	0.845 (0.0161)*
SN	0.869	0.794 (0.1686)	0.833 (0.4908)	0.836 (0.5103)	0.853 (0.7447)	0.839 (0.5472)	0.853 (0.7447)

* *P* values indicate that there are statistically significant differences (*P* < 0.05) between RNFL thickness and M-volume AUROC. Delong's method was performed for comparison of AUROC curves. Values of *P* < 0.05 established statistical significance. The *P* values reported are FDR-corrected to control for multiple testing.

TABLE 8. Comparison of the Diagnostic Capabilities of RNFL Thickness Versus GCC-Volume Parameters Using SD-OCT in a Subgroup of Early Glaucoma Patients

Location	RNFL Thickness AUROC	GCC-Volume-12 AUROC (*P* value)*	GCC-Volume-23 AUROC (*P* value)*	GCC-Volume-34 AUROC (*P* value)*	GCC-Volume-45 AUROC (*P* value)*	GCC-Volume-14 AUROC (*P* value)*	GCC-Volume-15 AUROC (*P* value)*
Global	0.934	0.810 (0.1427)	0.867 (0.1705)	0.901 (0.4409)	0.930 (0.9561)	0.885 (0.2391)	0.915 (0.6376)
Inferior	0.937	0.786 (0.0420)*	0.868 (0.1182)	0.896 (0.3314)	0.913 (0.5037)	0.877 (0.1613)	0.906 (0.4006)
Superior	0.882	0.806 (0.5111)	0.832 (0.5313)	0.850 (0.6358)	0.888 (0.9487)	0.854 (0.6881)	0.878 (0.9487)
Nasal	0.743	0.685 (0.6376)	0.760 (0.8919)	0.783 (0.6907)	0.807 (0.5457)	0.767 (0.8488)	0.791 (0.6376)
Temporal	0.740	0.872 (0.1580)	0.915 (0.0326)*	0.932 (0.0139)*	0.945 (0.0112)*	0.940 (0.0112)*	0.945 (0.0112)*
IT	0.919	0.824 (0.2036)	0.874 (0.2832)	0.892 (0.6119)	0.916 (0.9561)	0.890 (0.5166)	0.909 (0.8488)
IN	0.856	0.742 (0.2751)	0.805 (0.5543)	0.866 (0.8934)	0.888 (0.5910)	0.843 (0.8754)	0.877 (0.6881)
ST	0.872	0.817 (0.5925)	0.875 (0.9547)	0.880 (0.8934)	0.895 (0.6781)	0.897 (0.6554)	0.909 (0.5037)
SN	0.811	0.788 (0.8772)	0.782 (0.8052)	0.786 (0.8488)	0.818 (0.9487)	0.802 (0.9487)	0.817 (0.9487)

* *P* values indicate that there are statistically significant differences (*P* < 0.05) between RNFL thickness and GCC-volume AUROC. Delong's method was performed for comparison of AUROC curves. *P* values of < 0.05 established statistical significance. The *P* values reported are false discovery rate corrected (FDR-corrected) to control for multiple testing.

found that 100% of macular volume scans had at least one B-scan with an artifact. Overall study conclusions were that 3D datasets are better for patient care than 2D datasets, because 3D datasets afford the same or better diagnostic ability with fewer clinically significant testing artifacts.

The volume and thickness of the total macular retina and the inner macular retina (GCC) were calculated for six different-sized annular regions centered on the fovea (Fig. 2). Our study did not analyze the area bounded by the central circle of diameter of 1.00 mm, because the GCL is too thin to reliably measure at the foveal center. The area outside the 5-mm diameter circle was not analyzed, because an annulus with inner diameter of 5 mm and outer diameter of 6 mm would too frequently be outside the 6×6 mm² scanned region.

For all six annuli sizes, this study shows that all macular parameters were significantly reduced in glaucoma patients compared to normal subjects (*P* < 0.0001, Tables 4, 5). This is consistent with past time domain OCT and SD-OCT studies, which have also shown that the macula is thinner in glaucoma versus normal subjects.[6,14,24–26,45–54] In fact, glaucomatous damage is characterized by thinning of both the GCL and the RNFL, which represent 30% to 35% of the total macular thickness.[55] The current study also shows that the RNFL is thinner in glaucoma versus normal subjects for all regions (*P* < 0.0001, Table 3).

In the six annular regions studied, the AUROC or diagnostic capability of GCC-volume was significantly better compared to

M-volume in all corresponding regions (all *P* values between 0.0001 and 0.0445), except certain regions where GCC-volume AUROC were higher than but statistically similar to M-volume AUROC. This result is consistent with a study by Mori et al.[53] who used the RTVue SD-OCT (Optovue, Inc.) to analyze the central 5-mm diameter area of the macula, and who showed that the AUROC for GCC volume was significantly greater than the AUROC for total retinal volume in the same area (0.922 and 0.857, *P* = 0.020). Similarly, Kotowski et al.[26] used the Cirrus SD-OCT platform (Carl Zeiss Meditec, Inc.), which evaluates an elliptical annulus centered on the fovea with inner vertical radius of 0.5 mm and outer vertical radius of 2 mm, stretched horizontally by 20%, and found that the AUROC of GCIP and GCC thickness was significantly better than the AUROC of the total retinal thickness (AUROC average GCIP = 0.900, *P* = 0.016; AUROC average GCC = 0.901, *P* = 0.020; AUROC average retinal thickness [RT] = 0.839). Compared to the aforementioned studies,[26,53] our study design was different in that we used a different SD-OCT device (the Spectralis SD-OCT), we used a different scan protocol that utilizes a high density 6×6 mm macular volume scan, and we used our own novel custom-designed software which analyzed both total macular retina and GCC for both thickness and volume parameters for six modifiable annular regions.

Of all the 3D macular parameters, this study shows that GCC-volume-34 had the best diagnostic capability due to a combination of high AUROC curve values and of being within

TABLE 9. Comparison of the Diagnostic Capabilities of RNFL Thickness Versus M-Volume Parameters Using SD-OCT in a Subgroup of Early Glaucoma Patients

Location	RNFL Thickness AUROC	M-Volume-12 AUROC (*P* value)*	M-Volume-23 AUROC (*P* value)*	M-Volume-34 AUROC (*P* value)*	M-Volume-45 AUROC (*P* value)*	M-Volume-14 AUROC (*P* value)*	M-Volume-15 AUROC (*P* value)*
Global	0.934	0.691 (0.0112)*	0.774 (0.0302)*	0.806 (0.0438)*	0.830 (0.1022)	0.783 (0.0326)*	0.816 (0.0983)
Inferior	0.937	0.671 (0.0112)*	0.767 (0.0112)*	0.816 (0.0129)*	0.842 (0.0377)*	0.782 (0.0112)*	0.813 (0.0215)*
Superior	0.882	0.743 (0.1820)	0.767 (0.1958)	0.773 (0.1903)	0.786 (0.2301)	0.773 (0.2223)	0.781 (0.2268)
Nasal	0.743	0.621 (0.3654)	0.681 (0.6376)	0.722 (0.8785)	0.751 (0.9487)	0.692 (0.6781)	0.715 (0.8488)
Temporal	0.740	0.748 (0.9487)	0.796 (0.6344)	0.835 (0.3853)	0.835 (0.4006)	0.808 (0.5543)	0.816 (0.5166)
IT	0.919	0.680 (0.0112)*	0.798 (0.0231)*	0.840 (0.1022)	0.854 (0.2301)	0.811 (0.0326)*	0.835 (0.1022)
IN	0.856	0.631 (0.0300)*	0.735 (0.1748)	0.778 (0.3387)	0.813 (0.6373)	0.748 (0.2036)	0.772 (0.3654)
ST	0.872	0.766 (0.2755)	0.803 (0.4159)	0.799 (0.3390)	0.807 (0.3958)	0.813 (0.4975)	0.816 (0.5037)
SN	0.811	0.717 (0.5037)	0.724 (0.5037)	0.725 (0.5037)	0.740 (0.5543)	0.736 (0.5543)	0.739 (0.5543)

* *P* values indicate that there are statistically significant differences (*P* < 0.05) between RNFL thickness and M-volume AUROC. Delong's method was performed for comparison of AUROC curves. Values of *P* < 0.05 established statistical significance. The *P* values reported are FDR-corrected to control for multiple testing.

the 6 × 6 mm scanned region 100% of the time. When evaluating all six annular regions for GCC-volume, the best diagnostic capability was initially noted for overall GCC-volume-45, both for the entire group of OAG patients (Table 6) and for a subgroup of early OAG patients (Table 8). This initial interpretation would suggest that the most peripheral annulus (GCC-volume-45, with inner diameter of 4 mm and outer diameter of 5 mm) has the best diagnostic capability. This initial conclusion would also be consistent with previous studies that have shown that the peripheral macular regions are the most susceptible to glaucomatous damage.[6,25,51,53] However, one of the limitations of the most peripheral annulus, bound by diameters of 4 and 5 mm, is that the analyzed region is outside the 6 × 6 mm scanned square the highest percentage of the time, albeit only 0.9% of the time. In contrast, the GCC-volume-34 annular region was inside the square scanned region 100% of time and had some of the highest AUROC curve values (OAG patients: overall GCC-volume-34 = 0.939; temporal GCC-volume-34 = 0.947; IT GCC-volume-34 = 0.920, Table 6; early OAG patients: overall GCC-volume-34 = 0.901, temporal GCC-volume-34 = 0.932, inferior GCC-volume-34 = 0.896, IT GCC-volume-34 = 0.892, Table 8). Therefore, the best macular parameter for the clinical setting would be one where the annular region had high diagnostic capability but also was inside the scanned region 100% of the time (i.e., GCC-volume-34), to avoid the issue of incomplete datasets caused by decentered volume scans.

Of the four quadrants, the temporal GCC-volume-34 had the best diagnostic capability (OAG patients: 0.947, Table 6; early OAG patients: 0.932, Table 8). However, of the 4 sectors IT GCC-volume-34 had the best diagnostic capability (AUROC OAG patients: 0.920, Table 6; early OAG patients: 0.892, Table 8). These results are consistent with previous SD-OCT studies that showed that the macular regions most susceptible to glaucomatous changes are the inferior and temporal regions.[6-27,54,56] Tables 6, 7, 8, and 9 are also consistent with past studies,[27,28,30,32,35,36,54,57-61] in that Tables 6 through 9 show that the best diagnostic regions for RNFL thickness, aside from global RNFL thickness, are for the inferior and superior quadrants and for the IT and ST sectors (OAG patients: AUROC = 0.935–0.960; early OAG patients: AUROC = 0.872–0.937).

The RNFL thickness parameter is the most commonly used OCT parameter in glaucoma, but the diagnostic performance of GCC-volume-34 was similar to peripapillary RNFL thickness for overall global and for all quadrants and sectors, except for the temporal GCC-volume-34 that was significantly better than for temporal RNFL thickness (0.947 vs. 0.859, $P = 0.0067$, Table 6 for all glaucoma patients, and 0.932 vs. 0.740, $P = 0.0139$, Table 8 for early glaucoma patients). These results are in contrast to several past studies which showed better diagnostic capability for RNFL thickness compared to macular parameters assessed by RTVue-100 OCT.[35-37] These past studies suggest that the better diagnostic performance of the RNFL thickness parameter can be explained by the fact that 100% of the RGC axons can be measured by the peripapillary RNFL thickness parameter, while only 50% of RGCs contained in the human retina are concentrated within 4.5 mm of the fovea. In addition, macular measurements can be affected by nonglaucomatous diseases that independently affect macular thickness and volume. The current study suggests that macular volume scans may have advantages over RNFL thickness scans for diagnosis. In contrast to past studies that suggest that macular measurements are worse than RNFL thickness scans, this study's GCC-volume-34 parameter may have similar or better diagnostic abilities due to the high density volume scan (i.e., 193 B-scans over a 6 × 6 mm^2 region), in contrast to past studies which utilizes scan protocols of one horizontal line scan of 7 mm in length (467 A-scans) followed by 15 vertical

line scans of 7 mm in length (400 A-scans each) at 0.55-mm intervals.[35-37] Also, this high-density volume scan and associated custom-designed software may enable fewer clinically significant artifacts, thereby, enhancing diagnostic capability, especially in the temporal quadrant. Further studies are needed to test these hypotheses. Recent longitudinal studies also suggest that macular analysis may be better than or at least may complement RNFL measurements.[62,63] In a study by Kim et al.,[62] it was found that eyes with early glaucoma showed GC-IPL changes before corresponding peripapillary RNFL changes. Moon et al.[63] showed that serial GC-IPL measurements detected central glaucomatous functional progression as well as RNFL photographic assessment. Therefore, the current study and recent longitudinal studies suggest that macular analysis may play a more important role in the future for monitoring of glaucoma disease progression.

An objective of the current study was to analyze the artifact rates for 3D macular volume scans and to see if manual correction of artifacts is needed in the clinic. Even though 100% of macular volume scans had at least one B-scan with an artifact, manual correction of artifacts is not needed, because these artifacts did not significantly affect volume calculations (e.g., average difference between global GCC-volume values before and after correction was 0.005 ± 0.037 mm^3, where average GCC-volume-34 was 0.621 mm^3, Table 4, in this example, representing a 0.8% change in average values with correction). Also, the mean difference of the global M-thickness values before and after interpolation was 1.831 ± 20.658 μm. These differences are less than the 7 μm axial resolution of the Spectralis SD-OCT device.[64] These differences are also similar to or less than reported values for normal machine interscan variability for the central macular region (i.e., 0.46%[65] or 8.03 μm[66] to 15.0 μm[67]). Similarly, this study's volume scan artifacts did not affect diagnostic capability, because AUROC curve values for all 3D macular parameters for all annuli before and after interpolation did not significantly differ (i.e., P values between 0.8452 and 1.0000). When comparing our artifact rates with the literature, it is important to note that differences may be the result from whether artifact rates are reported as per B-scan or per volume scan. In this study, even though the artifact rate was 100% per volume scan (i.e., all volume scans had at least 1 B-scan with an artifact), Table 2 shows that artifact rates per B-scan ranged from 0.1% to 19.8%, with higher artifact rates in glaucoma versus normal subjects, and higher artifact rates for segmentation versus acquisition errors. Our artifact rate of 100% per volume scan with 193 B-scans is similar to a previous Spectralis study that analyzed macular volume scans in healthy patients and in subjects with retinal diseases.[39] In this study, Han and Jaffe[39] found that 90.9% of macular volume scans had at least one artifact, when volume scans were comprised of either 19 or 80 horizontal B-scans, with 1024 or 768 A-scans per line. In contrast, lower artifact rates were found when analyzing 2D data for artifact rates per B-scan, and both Asrani et al.[68] and Liu et al.[69] found that 19.9% and 46.3% of 2D RNFL thickness scans, respectively, had artifacts. Further studies are needed to compare the differing artifact rates for 2D versus 3D datasets and for the macula versus optic nerve and peripapillary regions. In summary, 3D volume scans appear less affected by artifacts compared to 2D B-scans, because occasional B-scan artifacts within volume scans can be adequately compensated for by neighboring artifact-free B-scans, such that final volume calculations are not significantly affected. In contrast, if an artifact is found in a single 2D B-scan, there are no neighboring B-scans to help correct for these errors and the 2D B-scan often can not be used clinically.

To better understand the types of artifacts in this study and in the aforementioned studies,[39,68,69] we grouped the artifacts

in two main categories: segmentation artifacts (i.e. misidentification or no segmentation of the ILM, GCC posterior boundary, or RPE), and acquisition artifacts (i.e., jump artifacts, cut edge artifacts, no image artifacts, or reflection error artifacts). In our study, we found that segmentation artifacts were more frequent than acquisition artifacts in both healthy and glaucoma subjects (2.6%–19.8% vs. 0.1%–0.5%, Table 2), suggesting that research into improved segmentation algorithms would be beneficial. In both glaucomatous and healthy subjects, the most frequent artifact was the segmentation artifact involving the posterior boundary of the GCC (i.e., 13.5% rate for healthy subjects and 19.8% rate for glaucoma patients, Table 2). These results agree with Han et al.[39] who found that the most frequent types of artifacts were misidentification of the inner (11.3%) and outer (13.2%) retina. The differences in the scattering proprieties of the inner macular layers are relatively small and not well resolved, and this can explain why the inner retinal layers are more difficult to segment. Han et al. also found higher rates of acquisition artifacts than we did (0.1%–9.3% vs. 0.1%–0.5%); this result can be explained by the fact that they studied patients with retinal diseases, where the anatomic alterations in the macular region and its associated visual impairments (i.e., fixation difficulties) can cause difficulties in image acquisition, compared to the healthy and glaucomatous subjects that we enrolled. This study similarly found that acquisition errors were higher in glaucoma patients compared to healthy patients (Table 2).

The current study has several limitations. The glaucoma subjects were older by an average of 14 years compared to the normal subjects (Table 1). Some studies have shown an age-related loss of retinal ganglion cells, and 7205 retinal ganglion cells are estimated to die per year.[70–72] Also, Pokharel et al.[73] showed that, with each year of increasing age, average macular thickness, and total macular volume decreases by 0.556 and 0.0156 mm^3 respectively. The age disparity between the glaucoma and control groups may have enhanced the diagnostic performance of the parameters investigated. However, it is important to highlight the fact that this limitation was overcome by the fact that the differences in macular and RNFL thickness as well as GCC volume between normal and glaucomatous subjects were far more than the expected for aging differences alone. More specifically, the expected difference of GCC-volume-34, for a 54.1-year-old normal person versus a 68.2-year-old normal person (14.1-year period) is about 0.007 mm^3; the actual difference in our study population comparing healthy and glaucomatous subjects was instead 0.163 mm^3. For macular thickness, the expected difference due to aging would be about 2.8 μm, while the actual difference between healthy and glaucomatous subjects was 27.9 μm. Finally, similar results have been obtained for RNFL thickness, which is known to thin physiologically by about 0.16 to 0.44 μm/year.[74–76] In our population, we found that the difference between healthy and glaucomatous subjects was about 36.5 μm, far more than the expected age-related decline of 1.2 μm. Considering the aforementioned results, it can therefore be concluded that age-matched normal controls and glaucoma patients were not needed. Another limitation of this study is that we did not do subgroup analysis of the diagnostic performance of these new macular parameters for preperimetric glaucoma or for all stages of disease severity, but only did analysis for all OAG patients and a subgroup with early OAG patients (VF MD: 0 to −6 dB). However, studies have shown that increased diagnostic capability occurs with increasing disease severity, so most past imaging studies have focused on the subset of early OAG patients when subgroup analysis was done. However, the results of our study can be only generalized to patients with perimetric glaucoma. Finally, in consideration of topographic studies which suggest that

temporal GCC volume should not just be compared to temporal RNFL thickness but also to superior-temporal and inferior-temporal RNFL thickness,[54] further studies are needed to better evaluate the diagnostic ability of 3D GCC parameters and 2D RNFL thickness after adjusting for the topographic correspondence shown by Hood et al.[54]

Finally, it is important to highlight that macular parameters measured by different SD-OCT devices may show different diagnostic abilities for glaucoma diagnosis. In details, the four most common SD-OCT platforms are represented nowadays by the Spectralis HRA OCT platform (Heidelberg Engineering), the RTVue SD-OCT platform (Optovue, Inc.), the Cirrus platform (Carl Zeiss Meditec), and the 3D OCT platform (Topcon, Inc., Tokyo, Japan). Each one of these platforms enables the assessment of the macular parameters with specific protocols that differentiate one device from the others. In details, the GCC scan protocol of the RTVue SD-OCT platform uses a 7-mm horizontal line with fifteen 7-mm vertical lines to display thickness values within a 6-mm diameter circle; the ganglion cell analysis of the Cirrus platform, measures the GCIPL in a 4.8 × 4.0 mm oval with a longer horizontal axis; the software PPAA in the Spectralis HRA OCT platform evaluates total retinal thickness in the macular region in a 30° × 25° scan region; 3D-OCT performs a raster scanning of a 7 mm^2 area centered on the fovea with a scan density of 512 (vertical) × 128 (horizontal) scans to derive the macular parameters. A study from Akashi et al.[77] comparing the diagnostic abilities of Cirrus, RTVue, and 3D-OCT for glaucoma, showed that the average GCC thicknesses measured using these OCT instruments exhibited similar diagnostic abilities. However, several studies comparing the diagnostic ability of the macular parameters to those of the traditional RNFL thickness with the different platforms showed contrasting results.[24–38] Specifically, studies using the Cirrus HD-OCT[26–30] and RTVue[31–34] instruments, comparing healthy subjects with patients with different stages of glaucoma, showed equivalent glaucoma diagnostic abilities of macular parameters (GCIPL or GCC, respectively) compared to peripapillary RNFL thickness (i.e., AUROC of the average GCIPL and GCC ranged from 0.735–0.964, and of average RNFL thickness from 0.735–0.972).[26–34] In other studies using RTVue OCT, average RNFL thickness performed better than the GCC in patients with preperimetric[35] and perimetric[36] glaucoma (i.e., AUROC of the average RNFL thickness ranged from 0.89035 to 0.91936 vs. 0.79035 to 0.86136 for GCC). Seong et al.[37] showed that GCC thickness had the same discriminating ability as peripapillary RNFL thickness for early glaucoma, while RNFL thickness performed better in patients with advanced disease. In our study, with the Spectralis platform, we showed that the best 3D macular parameter had the same or better diagnostic capability as 2D RNFL thickness. It is important to highlight that our results are not currently generalizable to other OCT systems which have different scan protocols and different commercially available software. Since one of our study aims was to develop new software that is customized not only for glaucoma but also for high-density scan protocols, these results could theoretically be generalizable to other OCT platforms if they were to use the same scan protocol and software. Future studies are needed to test this hypothesis.

In summary, this study showed that the best 3D macular parameter (GCC-volume-34) had the same or better diagnostic capability as 2D RNFL thickness. This study also demonstrated that inner retinal volume measurements (GCC-volume) had better diagnostic capability compared to total macular volume measurements (M-volume) for all annular regions analyzed. M-volume measurements had the same or worse diagnostic capability compared to RNFL thickness values. Lastly, artifacts are more common in glaucoma patients compared to normal

subjects, and 100% of macular volume scans had at least one B-scan with either an acquisition or segmentation artifact. However, manual deletion of erroneous frames with automated interpolation of the data did not increase the diagnostic capability of the macular parameters. Therefore, manual correction of macular volume scans is not necessary in the clinic, because artifacts are not clinically significant and, unlike RNFL thickness scans, can be compensated for by neighboring B-scans.

References

1. Quigley HA, Broman AT. The number of people with glaucoma worldwide in 2010 and 2020. *Br J Ophthalmol*. 2006;90:262–267.

2. Weinreb RN, Aung T, Medeiros FA. The pathophysiology and treatment of glaucoma: a review. *JAMA*. 2014;311:1901–1911.

3. Danias J, Shen F, Kavalarakis M, et al. Characterization of retinal damage in the episcleral vein cauterization rat glaucoma model. *Exp Eye Res*. 2006;82:219–228.

4. Huang D, Swanson EA, Lin CP, et al. Optical coherence tomography. *Science*. 1991;254:1178–1181.

5. Schuman JS, Pedut-Kloizman T, Hertzmark E, et al. Reproducibility of nerve fiber layer thickness measurements using optical coherence tomography. *Ophthalmology*. 1996;103:1889–1898.

6. Medeiros FA, Zangwill LM, Bowd C, Vessani RM, Susanna R Jr, Weinreb RN. Evaluation of retinal nerve fiber layer, optic nerve head, and macular thickness measurements for glaucoma detection using optical coherence tomography. *Am J Ophthalmol*. 2005;139:44–55.

7. Wollstein G, Schuman JS, Price LL, et al. Optical coherence tomography (OCT) macular and peripapillary retinal nerve fiber layer measurements and automated visual fields. *Am J Ophthalmol*. 2004;138:218–225.

8. Lederer DE, Schuman JS, Hertzmark E, et al. Analysis of macular volume in normal and glaucomatous eyes using optical coherence tomography. *Am J Ophthalmol*. 2003;135:838–843.

9. Wang M, Hood DC, Cho JS, et al. Measurement of local retinal ganglion cell layer thickness in patients with glaucoma using frequency-domain optical coherence tomography. *Arch Ophthalmol*. 2009;127:875–881.

10. DeBuc DC, Somfai GM, Ranganathan S, Tátrai E, Ferencz M, Puliafito CA. Reliability and reproducibility of macular segmentation using a custom-built optical coherence tomography retinal image analysis software. *J Biomed Opt*. 2009;14:064023.

11. Fabritius T, Makita S, Miura M, Myllylä R, Yasuno Y. Automated segmentation of the macula by optical coherence tomography. *Opt Express*. 2009;17:15659–15669.

12. Garvin MK, Abramoff MD, Kardon R, Russell SR, Wu X, Sonka M. Intraretinal layer segmentation of macular optical coherence tomography images using optimal 3-D graph search. *IEEE Trans Med Imaging*. 2008;27:1495–1505.

13. Garvin MK, Abramoff MD, Wu X, Russell SR, Burns TL, Sonka M. Automated 3-D intraretinal layer segmentation of macular spectral-domain optical coherence tomography images. *IEEE Trans Med Imaging*. 2009;28:1436–1447.

14. Ishikawa H, Stein DM, Wollstein G, Beaton S, Fujimoto JG, Schuman JS. Macular segmentation with optical coherence tomography. *Invest Ophthalmol Vis Sci*. 2005;46:2012–2017.

15. Kajic V, Povazay B, Hermann B, et al. Robust segmentation of intraretinal layers in the normal human fovea using a novel statistical model based on texture and shape analysis. *Opt Express*. 2010;18:14730–14744.

16. Mishra A, Wong A, Bizheva K, Clausi DA. Intra-retinal layer segmentation in optical coherence tomography images. *Opt Express*. 2009;17:23719–23728.

17. Quellec G, Lee K, Dolejsi M, Garvin MK, Abràmoff MD, Sonka M. Three-dimensional analysis of retinal layer texture identification of fluid-filled regions in SD-OCT of the macula. *IEEE Trans Med Imaging*. 2010;29:1321–1330.

18. Rossant F, Ghorbel I, Bloch I, Paques M, Tick S. Automated segmentation of retinal layers in OCT imaging and derived ophthalmic measures. *IEEE Trans Med Imaging*. 2009;28:1370–1373.

19. Yazdanpanah A, Hamarneh G, Smith B, et al. Intra-retinal layer segmentation in optical coherence tomography using an active contour approach. *Med Image Comput Comput Assist Interv*. 2009;12:649–656.

20. Curcio CA, Allen KA. Topography of ganglion cells in human retina. *J Comp Neurol*. 1990;300:5–25.

21. Kendell KR, Quigley HA, Kerrigan LA, Pease ME, Quigley EN. Primary open-angle glaucoma is not associated with photoreceptor loss. *Invest Ophthalmol Vis Sci*. 1995;36:200–205.

22. Wygnanski T, Desatnik H, Quigley HA, Glovinsky Y. Comparison of ganglion cell loss and cone loss in experimental glaucoma. *Am J Ophthalmol*. 1995;120:184–189.

23. Zeimer R, Asrani S, Zou S, Quigley H, Jampel H. Quantitative detection of glaucomatous damage at the posterior pole by retinal thickness mapping: a pilot study. *Ophthalmology*. 1998;105:224–231.

24. Pazos M, Dyrda AA Biarnés M, et al. Diagnostic accuracy of Spectralis SD OCT automated macular layers segmentation to discriminate normal from early glaucomatous eyes. *Ophthalmology*. 2017;124:1218–1228.

25. Kim HJ, Park KH, Kim YK, Jeoung JW. Evaluation of layer-by-layer segmented ganglion cell complex thickness for detecting early glaucoma according to different macular grids. *J Glaucoma*. 2017;26:712–717.

26. Kotowski J, Folio LS, Wollstein G, et al. Glaucoma discrimination of segmented cirrus spectral domain optical coherence tomography (SD-OCT) macular scans. *Br J Ophthalmol*. 2012;96:1420–1425.

27. Mwanza JC, Durbin MK, Budenz DL, et al. Glaucoma diagnostic accuracy of ganglion cell-inner plexiform layer thickness: comparison with nerve fiber layer and optic nerve head. *Ophthalmology*. 2012;119:1151–1158.

28. Jeoung JW, Choi YJ, Park KH, Kim DM. Macular ganglion cell imaging study: glaucoma diagnostic accuracy of spectral-domain optical coherence tomography. *Invest Ophthalmol Vis Sci*. 2013;54:4422–4429.

29. Takayama K, Hangai M, Durbin M, et al. A novel method to detect local ganglion cell loss in early glaucoma using

spectral-domain optical coherence tomography. *Invest Ophthalmol Vis Sci*. 2012;53:6904–6913.

30. Nouri-Mahdavi K, Nowroozizadeh S, Nassiri N, et al. Macular ganglion cell/inner plexiform layer measurements by spectral domain optical coherence tomography for detection of early glaucoma and comparison to retinal nerve fiber layer measurements. *Am J Ophthalmol*. 2013;156:1297–1307.

31. Moreno PA, Konno B, Lima VC, et al. Spectral-domain optical coherence tomography for early glaucoma assessment: analysis of macular ganglion cell complex versus peripapillary retinal nerve fiber layer. *Can J Ophthalmol*. 2011;46:543–547.

32. Rao HL, Babu JG, Addepalli UK, Senthil S, Garudadri CS. Retinal nerve fiber layer and macular inner retina measurements by spectral domain optical coherence tomograph in Indian eyes with early glaucoma. *Eye*. 2012;26:133–139.

33. Schulze A, Lamparter J, Pfeiffer N, Berisha F, Schmidtmann I, Hoffmann EM. Diagnostic ability of retinal ganglion cell complex, retinal nerve fiber layer, and optic nerve head measurements by Fourier-domain optical coherence tomography. *Graefes Arch Clin Exp Ophthalmol*. 2011;249:1039–1045.

34. Kim NR, Lee ES, Seong GJ, Kim JH, An HG, Kim CY. Structure-function relationship and diagnostic value of macular ganglion cell complex measurement using Fourier-domain OCT in glaucoma. *Invest Ophthalmol Vis Sci*. 2010;51:4646–4651.

35. Lisboa R, Paranhos A Jr, Weinreb RN, Zangwill LM, Leite MT, Medeiros FA. Comparison of different spectral domain OCT scanning protocols for diagnosing preperimetric glaucoma. *Invest Ophthalmol Vis Sci*. 2013;54:3417–3425.

36. Huang JY, Pekmezci M, Mesiwala N, Kao A, Lin S. Diagnostic power of optic disc morphology, peripapillary retinal nerve fiber layer thickness, and macular inner retinal layer thickness in glaucoma diagnosis with Fourier domain optical coherence tomography. *J Glaucoma*. 2011;20:87–94.

37. Seong M, Sung KR, Choi EH, et al. Macular and peripapillary retinal nerve fiber layer measurements by spectral domain optical coherence tomography in normal-tension glaucoma. *Invest Ophthalmol Vis Sci*. 2010;51:1446–1452.

38. Dave P, Shah J. Diagnostic accuracy of posterior pole asymmetry analysis parameters of Spectralis optical coherence tomography in detecting early unilateral glaucoma. *Indian J Ophthalmol*. 2015;63:837–842.

39. Han IC, Jaffe GJ. Evaluation of artifacts associated with macular spectral-domain optical coherence tomography. *Ophthalmology*. 2010;117:1177–1189.

40. Wu H, de Boer JF, Chen TC. Diagnostic capability of spectral-domain optical coherence tomography for glaucoma. *Am J Ophthalmol*. 2012;153:815–826.

41. Gordon MO, Kass MA. The Ocular Hypertension Treatment Study: design and baseline description of the participants. *Arch Ophthalmol*. 1999;117:573–583.

42. Cense B, Nassif N, Chen T, et al. Ultrahigh-resolution high-speed retinal imaging using spectral-domain optical coherence tomography. *Opt Express*. 2004;12:2435–2447.

43. Chen TC, Cense B, Pierce MC, et al. Spectral domain optical coherence tomography: ultra-high speed, ultra-high resolution ophthalmic imaging. *Arch Ophthalmol*. 2005;123:1715–1720.

44. Heidelberg Engineering. *Spectralis HRA+OCT User Guide Software Version 5.1*. Carlsbad, CA: Heidelberg Engineering GmbH; 2009.

45. Giovannini A, Amato G, Mariotti C. The macular thickness and volume in glaucoma: an analysis in normal and glaucomatous eyes using OCT. *Acta Ophthalmol Scand Suppl*. 2002;236:34–36.

46. Guedes V, Schuman JS, Hertzmark E, et al. Optical coherence tomography measurement of macular and nerve fiber layer thickness in normal and glaucomatous human eyes. *Ophthalmology*. 2003;110:177–189.

47. Lederer DE, Schuman JS, Hertzmark E, et al. Analysis of macular volume in normal and glaucomatous eyes using optical coherence tomography. *Am J Ophthalmol*. 2003;135:838–843.

48. Greenfield DS, Bagga H, Knighton RW. Macular thickness changes in glaucomatous optic neuropathy detected using optical coherence tomography. *Arch Ophthalmol*. 2003;121:41-46.

49. Wollstein G, Schuman JS, Price LL, et al. Optical coherence tomography (OCT) macular and peripapillary retinal nerve fiber layer measurements and automated visual fields. *Am J Ophthalmol*. 2004;138:218–225.

50. Wollstein G, Ishikawa H, Wang J, Beaton SA, Schuman JS. Comparison of three optical coherence tomography scanning areas for detection of glaucomatous damage. *Am J Ophthalmol*. 2005;139:39–43.

51. Ojima T, Tanabe T, Hangai M, et al. Measurement of retinal nerve fiber layer thickness and macular volume for glaucoma detection using optical coherence tomography. *Jpn J Ophthalmol*. 2007;51:197–203.

52. Tan O, Li G, Lu AT, Varma R, Huang D; Advanced Imaging for Glaucoma Study Group. Mapping of macular substructures with optical coherence tomography for glaucoma diagnosis. *Ophthalmology*. 2008;115:949–956.

53. Mori S, Hangai M, Sakamoto A, Yoshimura N. Spectral-domain optical coherence tomography measurement of macular volume for diagnosing glaucoma. *J Glaucoma*. 2010;19:528-34.

54. Hood DC, Razaa AS, de Moraesd CGV, Liebmannd JM, Ritchd R. Glaucomatous damage of the macula. *Prog Retin Eye Res*. 2013;32C:1–21.

55. Zeimer R, Shahidi M, Mori M, Zou S, Asrani S. A new method for rapid mapping of the retinal thickness at the posterior pole. *Invest Ophthalmol Vis Sci*. 1996;37:1994–2001.

56. Nakatani Y, Higashide T, Ohkubo S, Takeda H, Sugiyama K. Evaluation of macular thickness and peripapillary retinal nerve fiber layer thickness for detection of early glaucoma using spectral domain optical coherence tomography. *J Glaucoma*. 2011;20:252–259.

57. Mwanza JC, Oakley JD, Budenz DL, Anderson DR; The Cirrus OCT Normative Database Study Group. Ability of CirrusTM HD-OCT optic nerve head parameters to discriminate normal from glaucomatous eyes. *Ophthalmology*. 2011;118:241–248.e1.

58. Simavli H, Que CJ, Akduman M, Rizzo JL et al. Diagnostic capability of peripapillary retinal thickness in glaucoma using 3D volume scans. *Am J Ophthalmol*. 2015;159:545–556.

59. Mwanza JC, Budenz DL, Godfrey DG, et al. Diagnostic performance of optical coherence tomography ganglion cell-inner plexiform layer thickness measurements in early glaucoma. *Ophthalmology*. 2014;121:849–854.

60. Rao HL, Addepalli UK, Chaudhary S, et al. Ability of different scanning protocols of spectral domain optical coherence tomography to diagnose preperimetric glaucoma. *Invest Ophthalmol Vis Sci*. 2013;54:7252–7257.

61. Jeoung JW, Park KH. Comparison of Cirrus OCT and Stratus OCT on the ability to detect localized retinal nerve fiber layer defects in preperimetric glaucoma. *Invest Ophthalmol Vis Sci*. 2010;51:938–945.

62. Kim YK, Ha A, Na KI, Kim HJ, Jeoung JW, Park KH. Temporal relation between macular ganglion cell-inner plexiform layer loss and peripapillary retinal nerve fiber layer loss in glaucoma. *Ophthalmology*. 2017;124:1056–1064.

63. Moon H, Lee JH, Sung KR, Lee JE. Macular ganglion cell layer assessment to detect glaucomatous central visual field progression. *Korean J Ophthalmol*. 2016;30:451–458.

64. Heidelberg Engineering. *Spectralis HRA + OCT User Manual Software Version 5.7*. Carlsbad, CA: Heidelberg Engineering GmbH; 2013.

65. Wolf-Schnurrbusch UE, Ceklic L, Brinkmann CK, et al. Macular thickness measurements in healthy eyes using six different optical coherence tomography instruments. *Invest Ophthalmol Vis Sci*. 2009;50:3432–3437.

66. Comyn O, Heng LZ, Ikeji F, et al. Repeatability of Spectralis OCT measurements of macular thickness and volume in diabetic macular edema. *Invest Ophthalmol Vis Sci*. 2012;53: 7754–7759.

67. Ctori I, Huntjens B. Repeatability of foveal measurements using Spectralis optical coherence tomography segmentation software. *PLoS One*. 2015;10:e0129005.

68. Asrani S, Essaid L, Alder BD, Santiago-Turla C. Artifacts in spectral-domain optical coherence tomography measurements in glaucoma. *JAMA Ophthalmol*. 2014;132:396–402.

69. Liu Y, Simavli H, Que CJ, et al. Patient characteristics associated with artifacts in Spectralis optical coherence tomography imaging of the retinal nerve fiber layer in glaucoma. *Am J Ophthalmol*. 2015;159:565–576.

70. Balazsi AG, Rootman J, Drance SM, Schulzer M, Douglas GR. The effect of age on the nerve fiber population of the human optic nerve. *Am J Ophthalmol*. 1984;97:760–766.

71. Kerrigan-Baumrind LA, Quigley HA, Pease ME, Kerrigan DF, Mitchell RS. Number of ganglion cells in glaucoma eyes compared with threshold visual field tests in the same persons. *Invest Ophthalmol Vis Sci*. 2000;41:741–748.

72. Harwerth RS, Wheat JL, Rangaswamy NV. Age-related losses of retinal ganglion cells and axons. *Invest Ophthalmol Vis Sci*. 2008;49:4437–4443.

73. Pokharel A, Shrestha GS, Shrestha JB. Macular thickness and macular volume measurements using spectral domain optical coherence tomography in normal Nepalese eyes. *Clin Ophthalmol*. 2016;10:511–519.

74. Wu Z, Saunders LJ, Zangwill LM, Daga FB, Crowston JG, Medeiros FA. Impact of normal aging and progression definitions on the specificity of detecting retinal nerve fiber layer thinning. *Am J Ophthalmol*. 2017;181:106–113.

75. Leung CK, YE C, Weinreb RN, Yu M, Lai G, Lam DS. Impact of age-related change of retinal nerve fiber layer and macular thicknesses on evaluation of glaucoma progression. *Ophthalmology*. 2013;120:2485–2492.

76. Leung CKS, Yu M, Weinreb RN, et al. Retinal nerve fiber layer imaging with spectral-domain optical coherence tomography. a prospective analysis of age-related loss. *Am J Ophthalmol*. 2012;119:731–737.

77. Akashi A, Kanamori A, Nakamura M, Fujihara M, Yamada Y, Negi A. Comparative assessment for the ability of Cirrus, RTVue, and 3D-OCT to diagnose glaucoma. *Invest Ophthalmol Vis Sci*. 2013;54:4478–4484.